2nd IAA Conference on Space Situational Awareness (ICSSA)

Washington D.C., USA

IAA-ICSSA-20-0X-XX

Recent Radar Observations of the Sub-Centimeter Orbital Debris Environment

Timothy Kennedy[(1)]**, James Murray**[(2)]**, and Rossina Miller**[(2)]

[(1)]*NASA Johnson Space Center, 2101 NASA Pkwy XI511, Houston, TX 77058, timothy.f.kennedy@nasa.gov*

[(2)]*Jacobs, NASA Johnson Space Center, 2101 NASA Pkwy XI5-9E, Houston, TX 77058*

Keywords: *Radar, Orbital Debris, RSO, LEO*

1. Introduction

The NASA Orbital Debris Program Office (ODPO) has conducted radar observations of the orbital debris environment since the early 1990's to provide measurement data that supports orbital debris models and risk mitigation activities in support of NASA mission objectives. Orbital debris radar observations are a unique mode for radar operation, employing a fixed beam configuration to statistically sample the environment. An advantage of conducting operations in this fashion is that it enables observations of smaller classes of orbital debris than would otherwise be available from the same sensor operating in a traditional tracking mode. Orbital debris-mode radar observations are used to fill in the gaps, which exist in the currently available data from the Space Surveillance Network (SSN), on small size orbital debris populations that represent significant risk to NASA programs. These gaps have typically covered orbital debris with characteristic sizes less than approximately 10 cm down to approximately 3 mm in low Earth orbit (LEO) – depending upon the altitude and sensor configuration.

The value of orbital debris radar measurements lies in the ability to extract partial orbital element information about orbital debris in the centimeter to several millimeter size regimes in low Earth orbit – which are not available from other measurement sources. This paper will discuss observations of this smaller class of orbital debris observed in recent years from the radars at the MIT Haystack Observatory in Westford, Massachusetts, and the Goldstone Solar System Radar near Barstow, California. The former radar is able to observe orbital debris down to approximately 5 mm, and the latter, orbital debris with characteristic sizes near 3 mm – at altitudes less than 1000 km. The characteristics and inferences about the current LEO orbital debris environment, and the different subpopulations that are identifiable in the observations are highlighted.

2. Radar System Overview

Radar observations considered in this paper were collected from the Haystack Ultra-wideband Satellite Imaging Radar (HUSIR) over the U.S. Government fiscal years (FY) 2014 – 2017, as well as by the Goldstone Solar System Radar over the calendar years (CY) 2016 – 2017. The location for both of these radars are summarized in Table 1. Both radars are operated in a fixed beam or staring mode, where the radars are pointed to a particular elevation and azimuth angle, and data is sampled from the orbital debris (OD) environment by taking measurements of OD as it travels through the volume of space observed by the radar [1 – 2].

Table 1. HUSIR and Goldstone Location with respect to the 1984 World Geodetic System (WGS 84) Earth model.

Radar	Latitude	Longitude	Elevation
HUSIR	42.623287° N	288.511846° E	115.69 m
Goldstone	35.425901° N	243.110464° E	1002.11 m

Both HUSIR and Goldstone are extremely sensitive, with the common sensitivity metric being the signal-to-noise ratio (SNR) that is obtained with the radar from a conducting sphere having a radar cross section (RCS) of 0 dBsm. Using this metric, HUSIR and Goldstone have sensitivities of approximately 59.2 dB and 67.7 dB respectively.

HUSIR is a monostatic radar that uses a 36.6 m diameter Cassegrain reflector for both the transmit and receive antenna. Goldstone is a bistatic radar that uses a 70 m diameter Cassegrain reflector for the transmit antenna, and a 34 m diameter Cassegrain reflector for the receive antenna. The approximate normalized one-way radiation patterns for each antenna system are shown in Figure 1. Based on the radiation patterns shown in Figure 1, HUSIR has a 0.058° two-sided 3 dB beamwidth, while Goldstone has an approximate combined (70 m and 34 m bistatic array) two-sided 3 dB beamwidth of 0.037°.

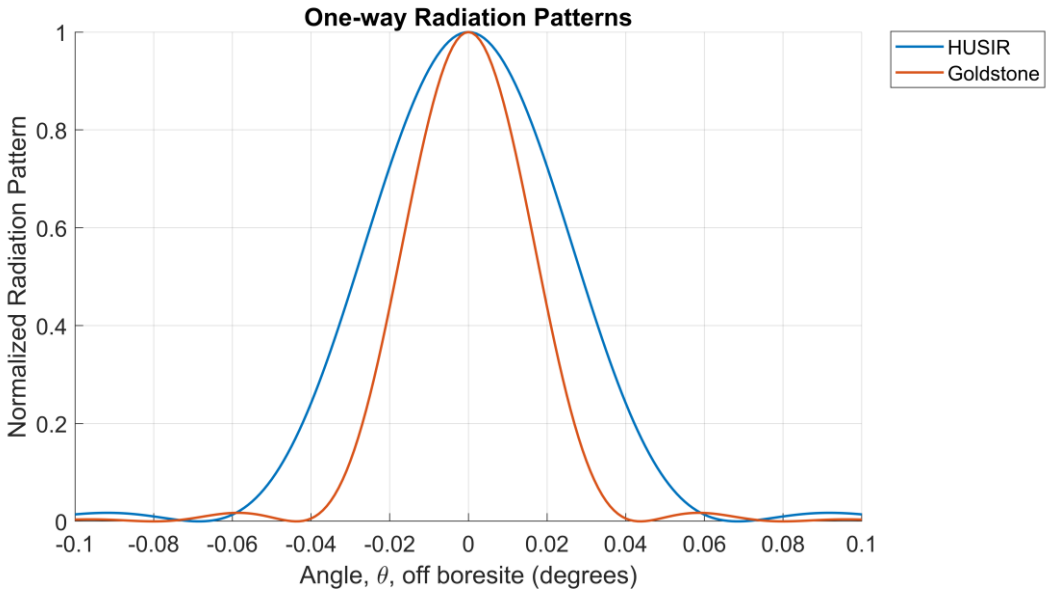

Figure 1. Approximate normalized radiation patterns for HUSIR and Goldstone, constructed using an Airy-disk approximation.

Since HUSIR and Goldstone both operate in a staring mode for orbital debris data collection, as the Earth rotates during operations, they both sample orbital debris passing through a thin shell, as indicated in Figure 2 for a given pointing, that determines the orbits that may be observed by each radar. In Figure 2, the thin shell depicted is for the configuration where each radar is pointed to an elevation angle of 75° and an azimuth that is due East, referred to as 75E. In the 75E pointing configuration, orbital debris inclinations that may be observed are restricted to inclinations with a lower bound approximately equal to the latitudes of each radar. Lower inclinations may be observed by pointing the radar to a lower elevation angle, similar to that shown in Figure 3, where HUSIR is pointed to an elevation of 20° and due South, referred to as 20S. The drawback to the latter pointing is that the slant range increases for observing orbital debris at a given altitude, so for observing the sub-centimeter orbital debris population at higher altitudes, the 75E pointing is required.

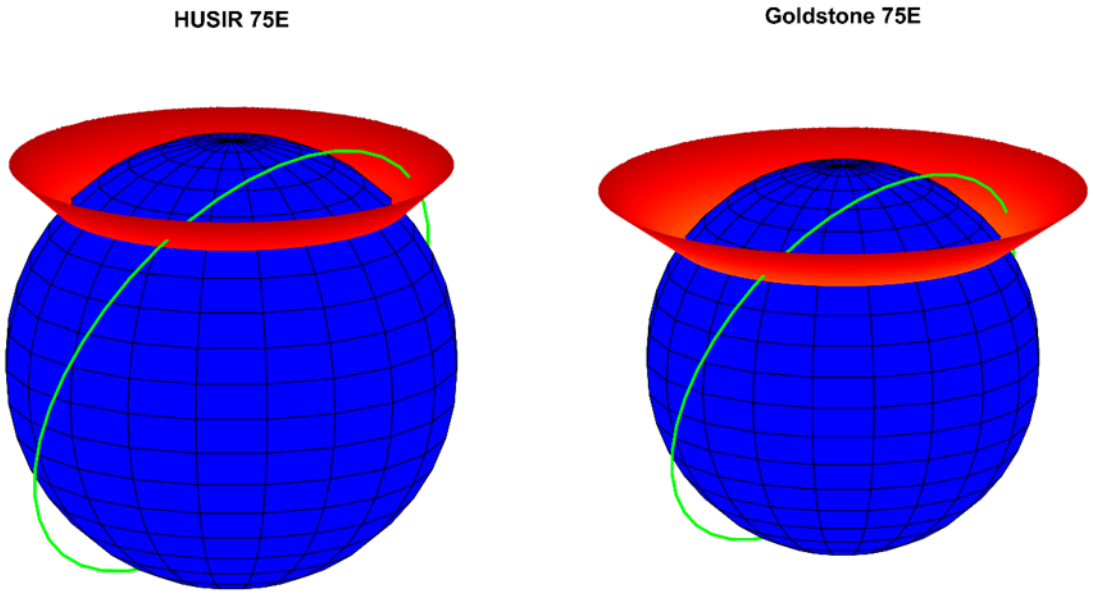

Figure 2. Thin shells (in red) sampled by the HUSIR and Goldstone radars as their beams are swept in time. A reference circular orbit is shown in green, for an altitude of 800 km and an inclination of 65 degrees.

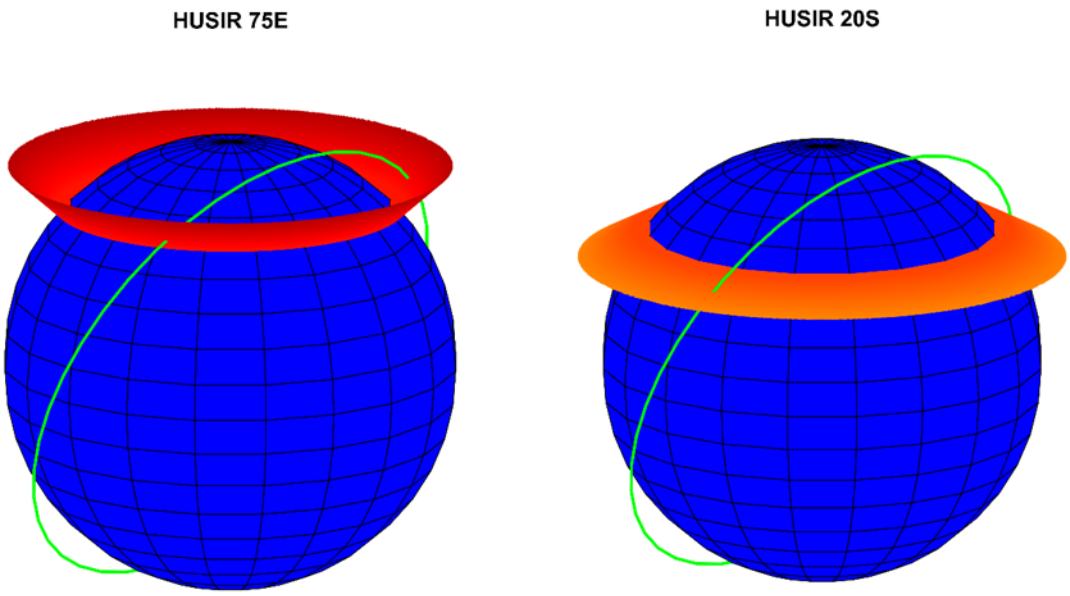

Figure 3. Thin shells (in red and orange) sampled by the HUSIR 75E and 20S pointing geometries. A reference circular orbit is shown in green, for an altitude of 800 km and an inclination of 65 degrees.

3. Measurements

A high-level summary of the observation hours, total number of detections, and average count rates per year for the HUSR and Goldstone radars are shown in Table 2. The average count rate for Goldstone in 2017 is lower than in 2016, which is due to lower transmitter power, 240 kW, in the latter part of 2017 relative to the nominal 440 kW that was available for all of 2016. This reduced the ability of Goldstone to detect smaller orbital debris objects, particularly at higher altitudes. A similar situation exists for HUSIR in 2017, where the transmitter power available was significantly below nominal throughout the year. Note that the average count rate for Goldstone is significantly higher than that for HUSIR. This is due to Goldstone's higher sensitivity, as well as the range window extending to 3373 km for Goldstone versus 2129 km for HUSIR – for the 75E pointing geometry.

Table 2. Summary of measurements taken by HUSIR in 2014 - 17 and Goldstone in 2016-17.

Radar	Year	Observation Hrs	Total Number of Detections	Average Count Rate
HUSIR 75E	2014	268.1	4107	15.3
HUSIR 75E	2015	288.4	4858	16.8
HUSIR 75E	2016	458.5	7079	15.4
HUSIR 75E	2017	496.2	5701	11.5
Goldstone 75E	2016	46.3	3427	74
Goldstone 75E	2017	51.8	3064	59.1

Direct measurements from both sensors are range, range-rate, the signal-to-noise ratio, and information on the polarization of the orbital debris detected. Numerous additional parameters are determined from these basic measurements, including information on the inclination. Assuming a circular orbit, the range and range-rate

measurements are transformed into altitude and Doppler inclination as shown in Figures 4 – 5. Based on the observations shown in these two figures, a number of important orbital debris families are evident. The heavily trafficked Sun-synchronous family is observable, clustered about the Sun-synchronous condition for circular orbits, which is indicated by the dashed black curve in both figures. Also of note are the Sodium-Potassium (NaK) coolant droplets, discussed in more detail in Section 5.

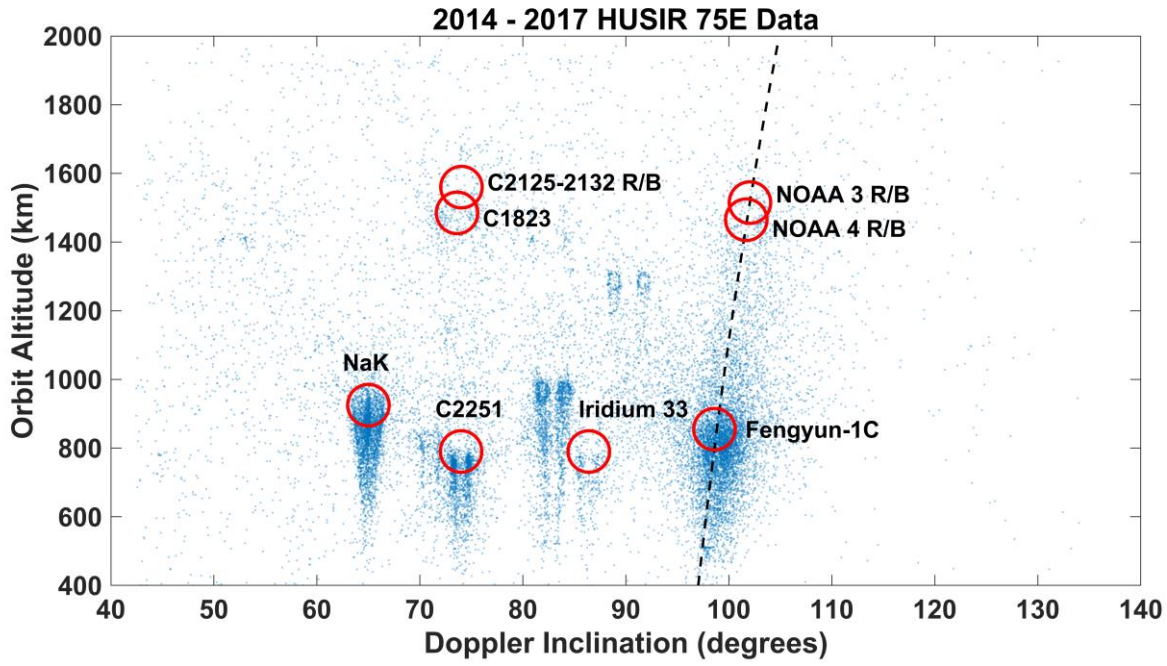

Figure 4. Orbit altitude versus average Doppler inclination for debris detected by HUSIR 75E in calendar year 2014-17.

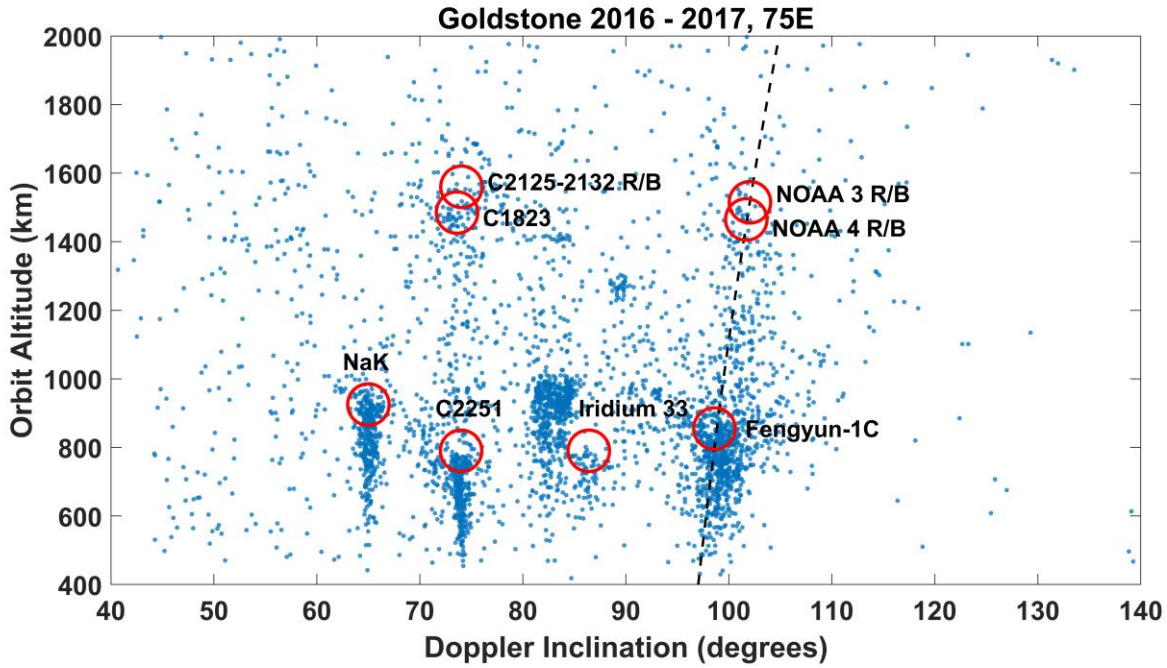

Figure 5. Orbit altitude versus average Doppler inclination for debris detected by Goldstone 75E in calendar year 2016-17.

4. The NASA Size Estimation Model

The NASA size estimation model (SEM) was developed to relate the radar cross section (RCS) of orbital debris to physical size. The SEM uses a characteristic length to summarize the physical size of an orbital debris object. Characteristic length is an average of the three largest dimensions of an object measured along three orthogonal axes. The first corresponds to the length of the largest dimension, denoted as X in Figure 6. The second is the longest projection measurement, Y, in a plane orthogonal to the first – also shown in Figure 6. The third dimension is chosen orthogonal to the first two dimensions – completing the orthogonal triad. Characteristic length is used interchangeably in reference to size or diameter of an object.

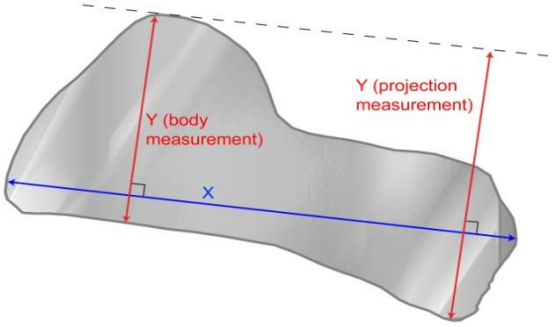

Figure 6. Illustration of body and projected measurement on complex shape used in determining characteristic length.

The results of RCS-to-size measurements on 39 representative debris objects are shown in Figure 7, where each point represents an average RCS over many orientations for a single object measured at a single frequency. The oscillating curve is the RCS for a spherical conductor while the smooth curve is the fit to the data and comprises the NASA SEM, which maps RCS to a characteristic length – or diameter [3 – 7].

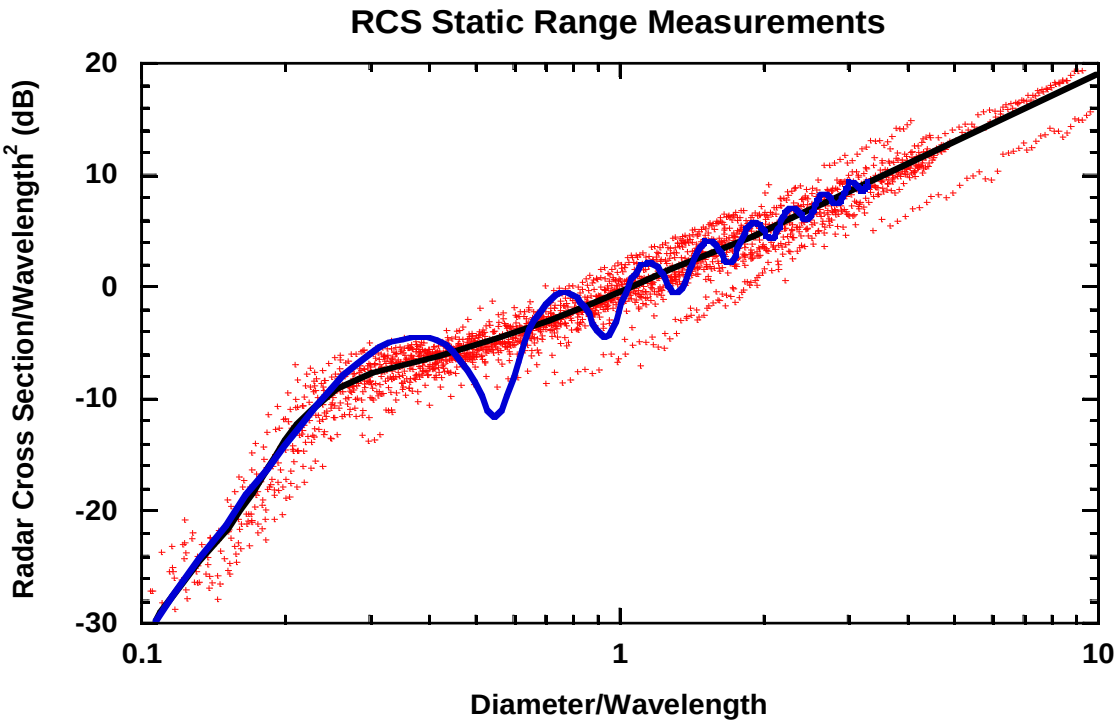

Figure 7. Results of RCS-to-size measurements on 39 representative debris objects. The oscillating line is the RCS for a spherical conductor while the smooth line is the fit to the data.

5. Radar Calibration Using Sodium-Potassium (NaK) Coolant Droplets

The NaK population is an excellent OD radar calibration source, which generally has stable count rates on a yearly basis [8]. Due to the formation of the NaK coolant droplets in the microgravity of orbit, this population consists of individual metallic spheres. As a result, this population may be examined by separating these spheres from the rest of the orbital debris population based on altitude, inclination, and polarization.

The empirical size distribution for the NaK is based on the work of Foster, and the presence of an inflection point in the distribution is largely independent of the details of the size distribution model selected [8 – 10]. Figure 8 details a model for the cumulative number of NaK particles as a function of the RCS at the HUSIR wavelength of 3 cm (10 GHz). An inflection point at –35 dBsm is indicated with the dashed vertical line. The location of this inflection point in RCS space is frequency dependent. This particular RCS value also corresponds to the peak in the Mie resonance region, shown in Figure 9, for Mie scattering for a sphere at the HUSIR center frequency of 10 GHz.

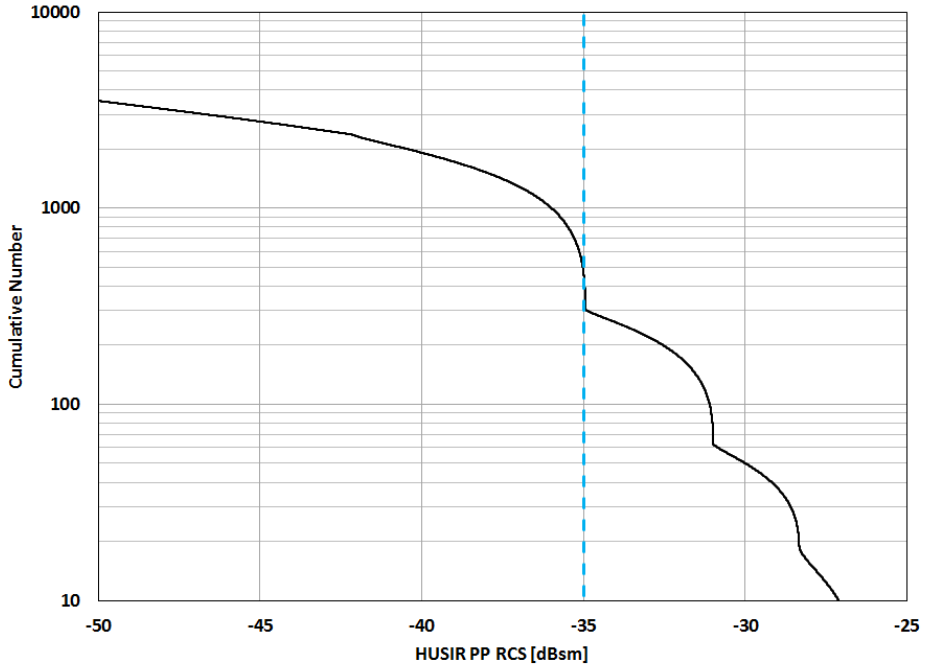

Figure 8. Model for the cumulative number of on-orbit NaK spheres vs RCS at the HUSIR wavelength (3 cm). An inflection point at -35 dBsm, which is frequency dependent, may be used for calibration at the HUSIR wavelength.

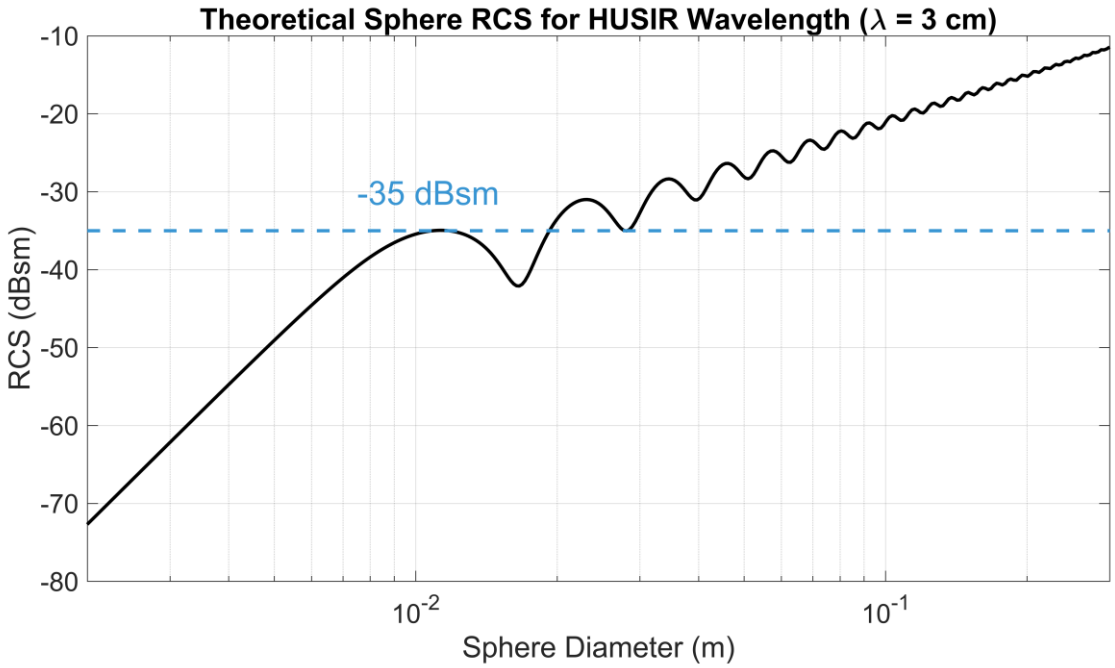

Figure 9. Mie scattering for spheres at the HUSIR X-band wavelength. A reference line at -35 dBsm is shown, which marks the peak in the Mie resonance region and the location of the inflection point in the cumulative count of the NaK.

A similar relation exists for the Goldstone radar, with a center frequency of 8.56 GHz. The peak of the Mie resonance region for this radar is near –33.6 dBsm, as shown in Figure 10. Unlike HUSIR, Goldstone does not have a monopulse receiver, and the path an object takes through the Goldstone beam introduces a bias for the true RCS measurement of an object. Examination of the NaK population and determining the correction needed in the observed size distribution to make the inflection point match

with the RCS of the Mie resonance peak may be used to adjust for this RCS bias. Application of this correction is typically conducted on an annual basis for Goldstone since the observation hours should be sufficient for the inflection point to be evident in the cumulative count distribution of the NaK population.

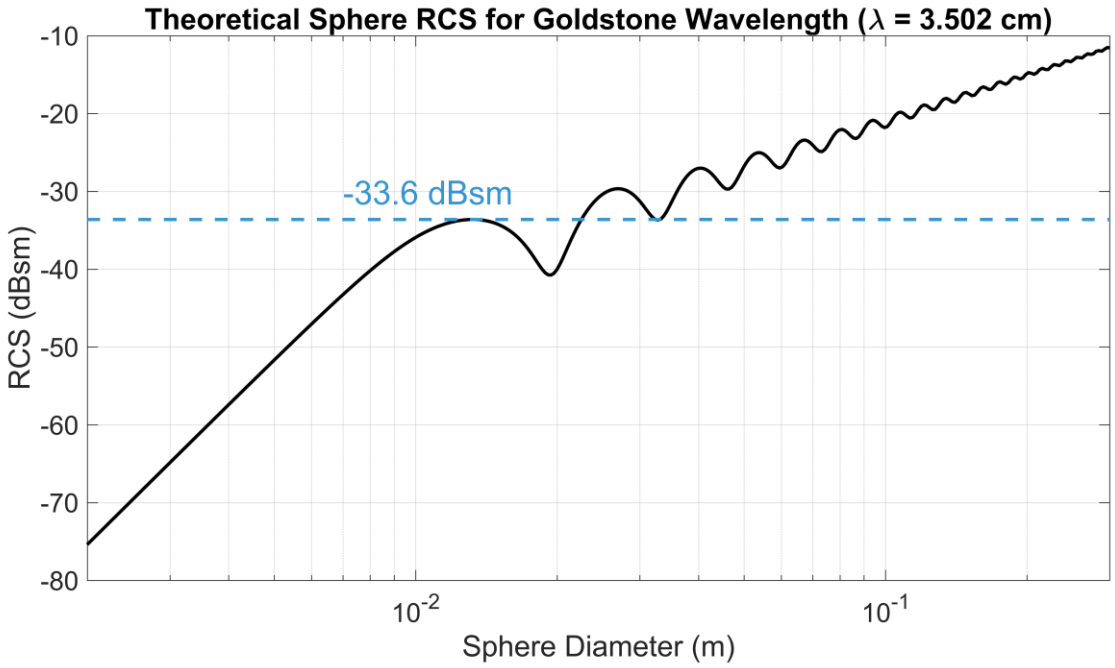

Figure 10. Mie scattering for spheres at the Goldstone X-band wavelength. A reference line at -33.6 dBsm is shown, which marks the peak in the Mie resonance region and the location of the inflection point in the cumulative count of the NaK.

6. Centimeter and Sub-Centimeter Orbital Debris (OD) Populations

To investigate the centimeter and sub-centimeter OD population in LEO, measured cumulative surface area flux is considered. This flux represents the cumulative number of orbital debris objects of a given size and larger that are observed per unit area per unit time by the radar. The cumulative flux observed by HUSIR over the calendar years 2014 – 17 is shown in Figure 11. The shaded regions indicate the 2σ Poisson uncertainties. The centimeter and sub-centimeter orbital debris flux shown is relatively stable over the years considered. The roll-off in the cumulative flux at smaller orbital debris sizes corresponds to the limit in sensitivity for HUSIR in a given calendar year. Hence, for years with nominal operations, HUSIR is able to observe objects approximately 5.5 mm and larger for altitudes below 1000 km. In 2017, the sensitivity was reduced as the result of a significant reduction in transmitter power that occurred in this year. This is the reason for the cumulative flux roll-off at slightly larger SEM sizes than in other years.

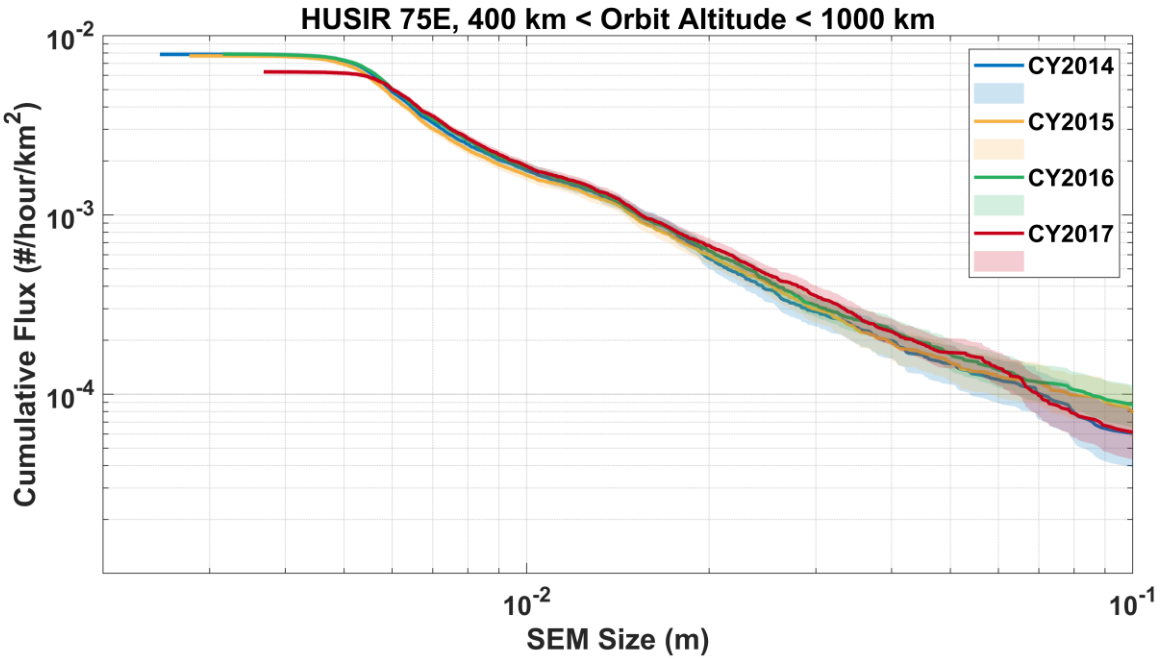

Figure 11. Cumulative surface area flux of orbital debris for altitudes in the range 400 - 1000 km for the HUSIR radar in 2014 - 2017. Shaded regions represent the 2σ Poisson uncertainties.

As described in Section 3, Goldstone is more sensitive and nominally operated with a longer-range extent than HUSIR. Limiting the data collected by Goldstone to the same altitude region, 400 – 1000 km, the surface area flux for both Goldstone and HUSIR during 2016-17 are considered in Figure 12. The 2σ Poisson uncertainties are again depicted using shaded regions of the same color as the yearly curves for each radar. Note that good agreement between the data collected by both radars is obtained, and that the Goldstone data extends the cumulative surface area flux curves to smaller orbital debris sizes than HUSIR.

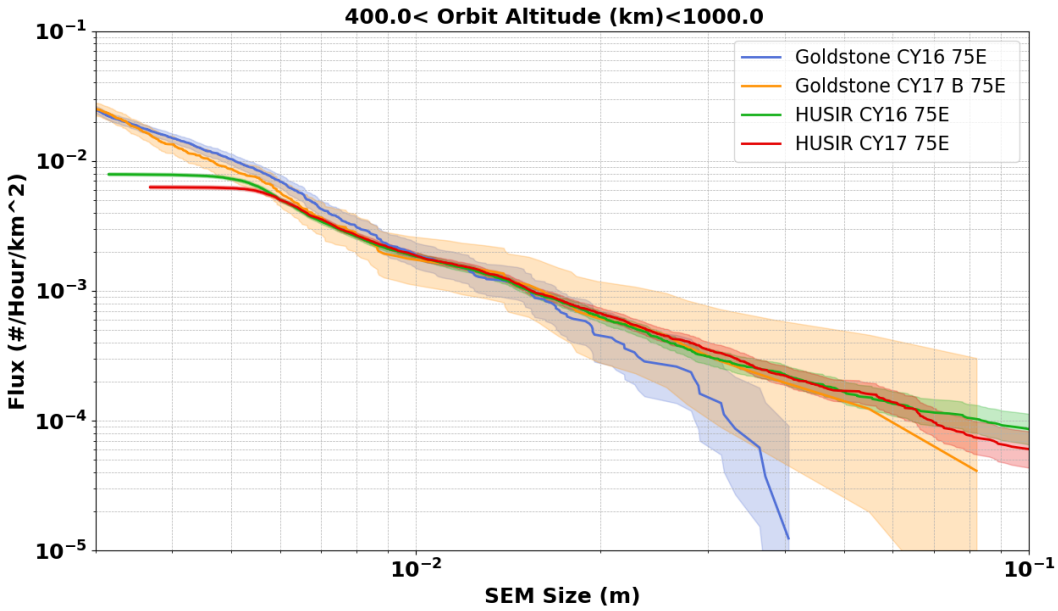

Figure 12. Cumulative surface area flux of orbital debris altitudes between 400 - 1000 km for the Goldstone and HUSIR radars in 2016 - 2017. Shaded regions represent the 2σ Poisson uncertainties.

Radar observations of the OD environment in LEO may be further examined by considering the surface area flux as a function of altitude. Observations for OD objects ≥ 1 cm are shown in Figure 13. Shaded regions indicate the 2σ Poisson uncertainties. The flux measurements generally have overlapping uncertainties from year-to-year, indicating that the surface area flux is relatively stable for the observational years considered. An upper limit of 1600 km in altitude is applied to the data in Figure 13 since in most years; this is the approximate altitude to which HUSIR is sensitive to the 1 cm population. A similar plot of surface area flux as a function of altitude is considered in Figure 14 for OD objects ≥ 5.5 mm. In the latter case, an altitude limit of 1000 km is applied to match HUSIR's approximate sensitivity for most years to the 5.5 mm population. Again, note that the environment is relatively stable for the observational years considered.

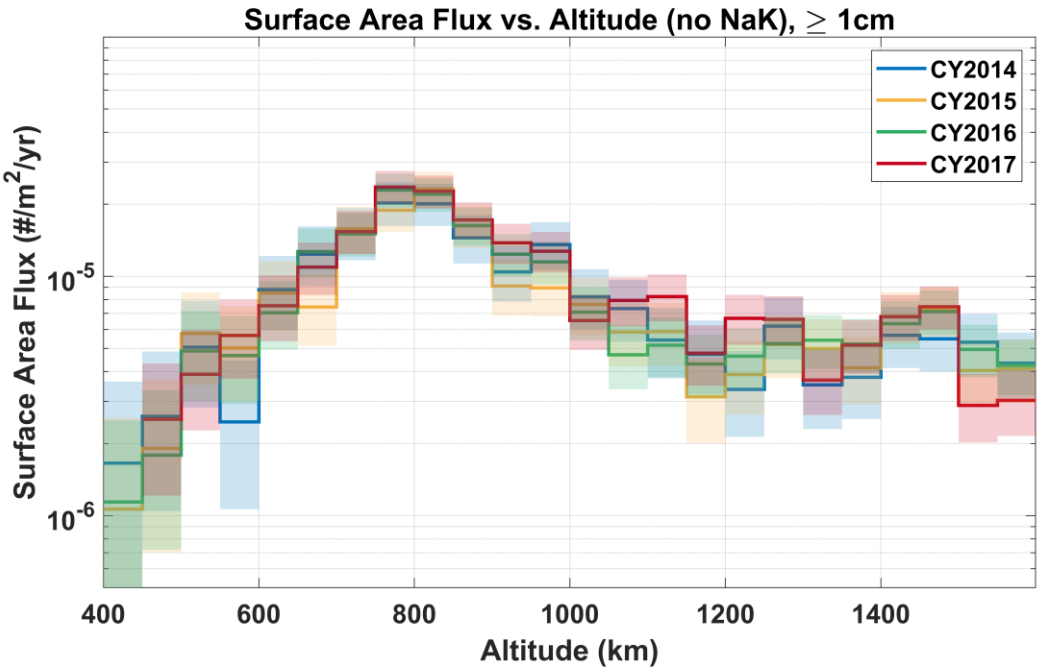

Figure 13. Cumulative surface area flux versus altitude for the ≥ 1 cm population (without NaK). Shaded regions indicate 2σ Poisson uncertainties.

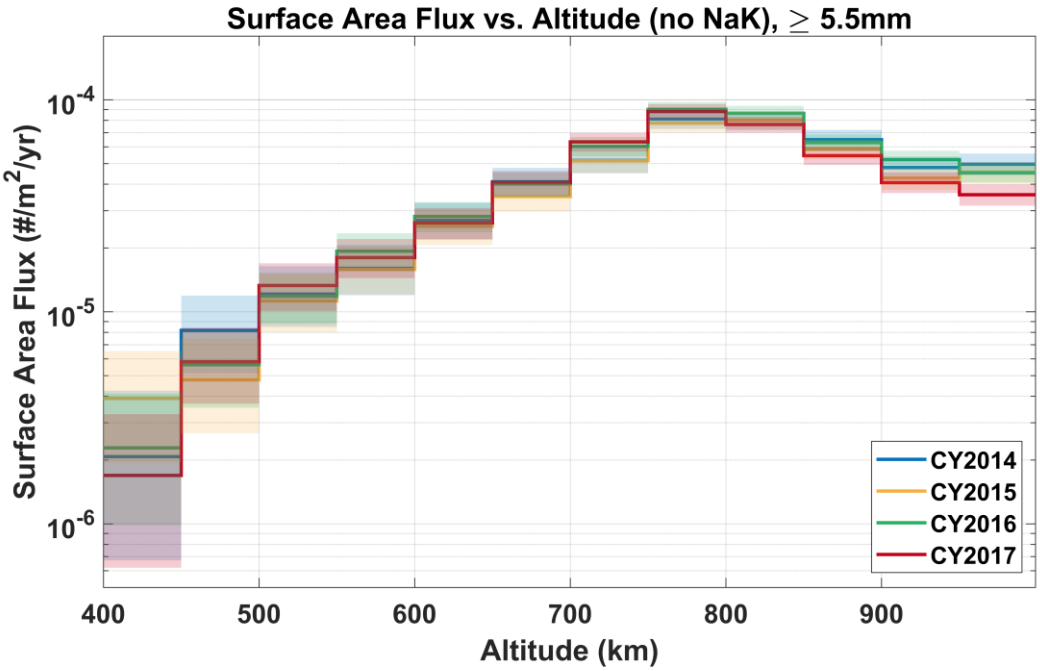

Figure 14. Cumulative surface area flux versus altitude for the ≥ 5.5 mm population (without NaK). Shaded regions indicate 2σ Poisson uncertainties.

7. Summary

This paper presented recent radar measurements of the centimeter and sub-centimeter LEO orbital debris environment. Both HUSIR and Goldstone radar measurements were considered. Detected orbital debris from these radars in all years considered directly measured range, range-rate, signal-to-noise ratio, and polarization information. Derived quantities from these measurements, e.g., Doppler inclination was discussed, and the clustering of OD into orbital families was observed

in altitude and inclination space. Calibration and validation of OD radar measurements using the NaK coolant droplets was discussed. The NaK population was shown to be useful for correcting RCS in radar measurements without a built-in method to determine the path that OD takes when traversing the radar beam.

The cumulative flux of the centimeter and sub-centimeter population, as a function of both size and altitude, were considered. The flux of this population was shown to be relatively stable over the observational years considered in this paper. Both the Goldstone and HUSIR radar measurements indicate similar OD flux for this population, down to a SEM size of approximately 5 mm. Measurements from Goldstone enabled flux measurements to be made down to approximately 3 mm for altitudes below 1000 km.

8. References

[1] Murray, J., Blackwell, C., Gaynor, J., *et al.*, "Haystack Ultra-Wideband Satellite Imaging Radar Measurements of the Orbital Debris Environment: 2014-2017," NASA/TP-2019-220302, 2019.

[2] Murray, J., Miller, R., Matney, M., *et al.*, "Recent Results from the Goldstone Orbital Debris Radar: 2016 – 2017," 1st International Orbital Debris Conference, Sugar Land, TX, December 2019.

[3] Dalquist, C. and Bohannon, G. "Physical Descriptions of Debris Objects Used in Static RCS Measurements," XonTech Report 910555-1978. August 1991.

[4] Bohannon, G., Caampued, T., and Young, N., "First Order RCS Statistics of Hypervelocity Impact Fragments," XonTech Report 940128-BE-2305. April, 1994.

[5] Barton, D. K., Brillinger, D., El-Shaarawi, A.H., *et al.*, "Final Report of the Haystack Orbital Debris Data Review Panel," NASA/JSC Technical Memorandum 4809, Houston, TX, February 1998.

[6] Everett, R., Caampued, T., and Chu, J., "Summary of Data Processing of September 1990 SPC Debris Data," XonTech Report 910147-1937, March 1991.

[7] Everett, R., Dalquist, C., and Caampued, T., "Summary of Processing of January 1991 SPC Debris Data," XonTech Report 9100393-1965, July 1991.

[8] Matney, M., Anz-Meador, P., Murray, J., *et al.*, "The NaK Population: A 2019 Status," 1st International Orbital Debris Conference, Sugar Land, TX, December 2019.

[9] Foster, J.L., Krisko, P., Matney, M., et al. "NaK Droplet Source Modeling." IAC-03-IAA.5.2.02, 2003.

[10] Krisko, P.H., and J.L. Foster. "Modeling the sodium potassium droplet interactions with the low earth orbit space debris environment," Acta Astronautica 60, pp. 939-945, 2007.